Astronomy & Astrophysics manuscript no. appendicesDJ
January 12, 2025

Gaia Data Release 3: Spectroscopic binary-star orbital solutions

The SB1 processing chain

E. Gosset[1,⋆], Y. Damerdji[2,1], T. Morel[1], L. Delchambre[1], J.-L. Halbwachs[3], G. Sadowski[4], D. Pourbaix[4,†⋆⋆], A. Sozzetti[5], P. Panuzzo[6], and F. Arenou[6]

[1] Institut d'Astrophysique et de Géophysique, Université de Liège, 19c, Allée du 6 Août, B-4000 Liège, Belgium
[2] CRAAG-Centre de Recherche en Astronomie, Astrophysique et Géophysique, Route de l'Observatoire, Bp 63 Bouzareah, DZ-16340 Algiers, Algeria
[3] Université de Strasbourg, CNRS, Observatoire Astronomique de Strasbourg, UMR 7550, 11 rue de l'Université, F-67000 Strasbourg, France
[4] Institut d'Astronomie et d'Astrophysique, Université Libre de Bruxelles CP 226, Boulevard du Triomphe, B-1050 Brussels, Belgium
[5] INAF - Osservatorio Astrofisico di Torino, via Osservatorio 20, I-10025 Pino Torinese (TO), Italy
[6] GEPI, Observatoire de Paris, Université PSL, CNRS, 5 Place Jules Janssen, F-92190 Meudon, France

Received 3 May 2024; accepted 8 October 2024

ABSTRACT

Context. The *Gaia* satellite constitutes one of ESA's cornerstone missions. Being primarily an astrometric space experiment measuring positions, proper motions, and parallaxes for a huge number of stars, it also performs photometric and spectrophotometric observations. *Gaia* operates a medium-dispersion spectrometer, known as Radial Velocity Spectrometer (RVS), which provides spectra and radial velocity (RV) time series.
Aims. The paper is focussed on the analysis of the RV time series. We fit orbital and trend models, restricting our study to objects of spectral types F-G-K that are brighter than a magnitude of 12, presenting only one single spectrum (SB1).
Methods. Suitable time series were processed and analysed on an object-per-object basis, providing orbital or trend solutions. The results of the various fits were further filtered internally on the basis of several quality measures to discard spurious solutions. The objects with solely a spectroscopic solution were classified in one of the three classes: `SB1` (eccentric model), `SB1C` (circular model), or `TrendSB1` (mere trend model).
Results. We detail the methods used in this work and describe the derived parameters and results. After a description of the models considered and the related quality tests of the fit, we detail the internal filtering process aimed at rejecting bad solutions. We also present a full validation of the pipeline. A description of the current content of the catalogue is also provided.
Conclusions. We present the `SB1`, `SB1C`, and `TrendSB1` spectroscopic solutions contained in the SB subcatalogue, part of the DR3 catalogue. We deliver some 181 327 orbital solutions in class `SB1`, 202 in class `SB1C`, and 56 808 in the associated class `TrendSB1`. This is a first release and the delivered SB subcatalogue could be further tuned and refined. However, the majority of the entries are correct. Thus, this data set constitutes by far the largest set of spectroscopic orbital solutions to be computed.

Key words. Techniques: spectroscopy; Stars: Techniques: radial velocities; Stars: binaries; Catalogues: Survey; Gaia

This document contains the Appendices D-J of the article Gosset et al. on *Gaia* NSS-SB1, see

Astronomy & Astrophysics, January 2025, 693, A124
DOI: `https://doi.org/10.1051/0004-6361/202450600`

⋆ Research Director, F.R.S.-FNRS (Belgium)
⋆⋆ † Deceased 2021

Appendix D: Pie charts illustrating the tallies

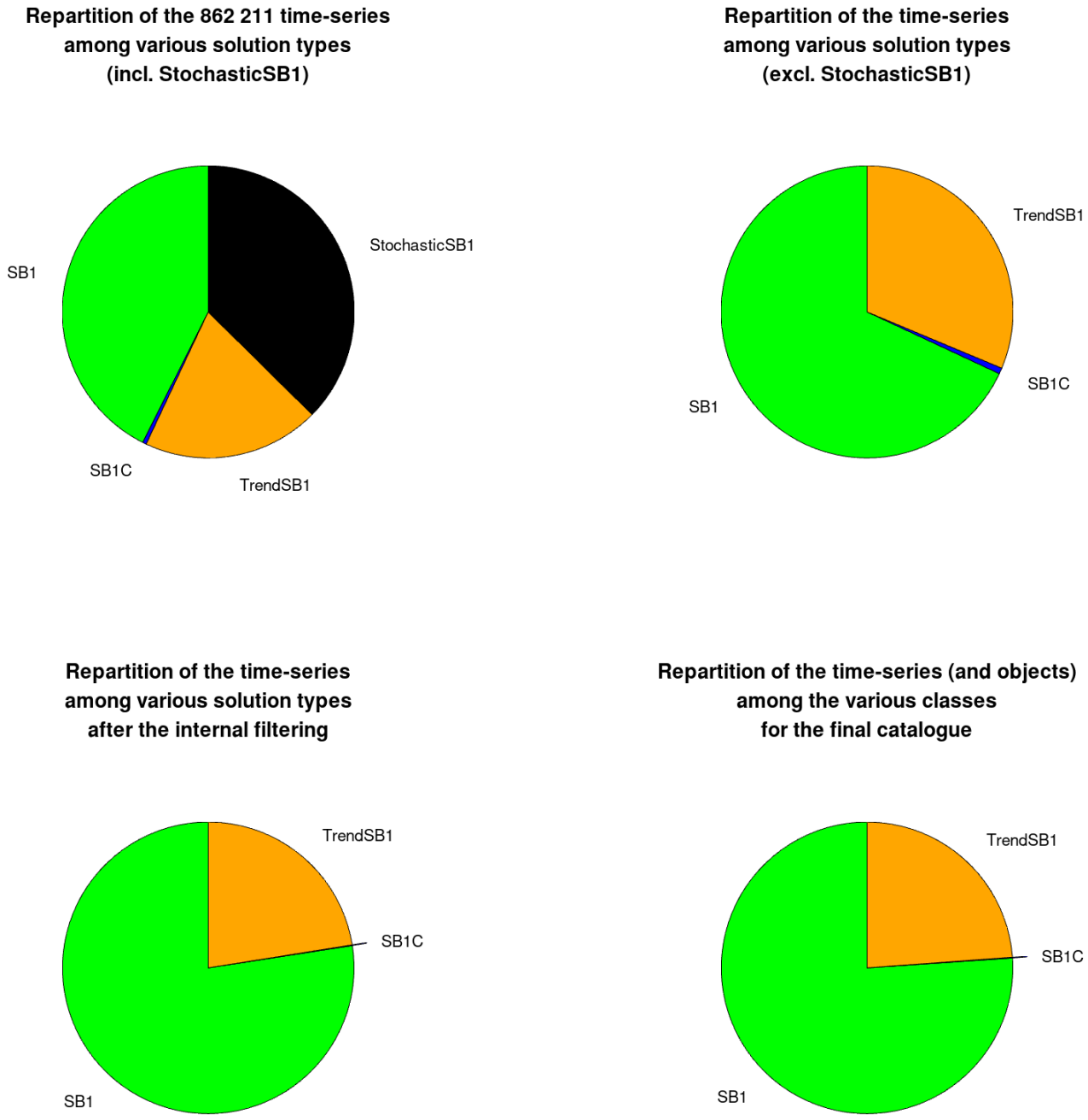

Fig. D.1: Pie charts illustrating (upper row) the repartition of the time-series among the various solution types including and excluding the StochasticSB1 (see Table 1) and its evolution (lower row) over the course of the various losses: internal filtering (left: Tables 2, 3, 4) and combination+post-filtering (right: Tables 6, 7, 8).

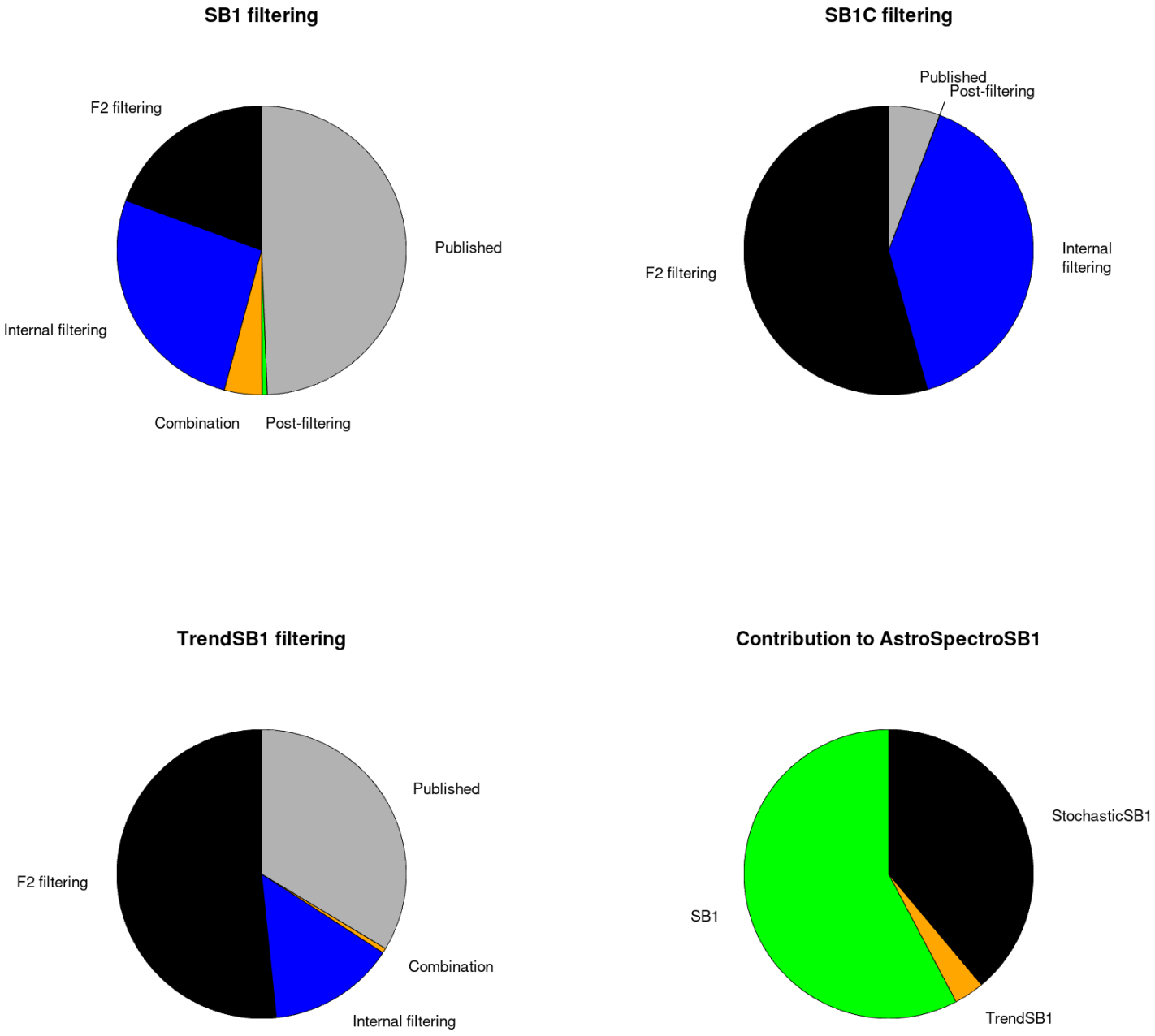

Fig. D.2: Details of the percentage of discarding at the various steps before publication for the SB1 solution type (upper left), for the SB1C solution type (upper right) and for the TrendSB1 solution type (lower left). The F_2 filtering is the first step of the internal filtering and its contribution is represented in black. The effect of the subsequent steps of the internal filtering is in blue. The effect of the loss by combination is in orange and the one of the post-filtering is in green. The gray sector represents the proportion published. The lower right pie chart gives the contribution of the different solution types to the `AstroSpectroSB1` class (see Table 9).

Appendix E: A few examples of resulting orbital solutions

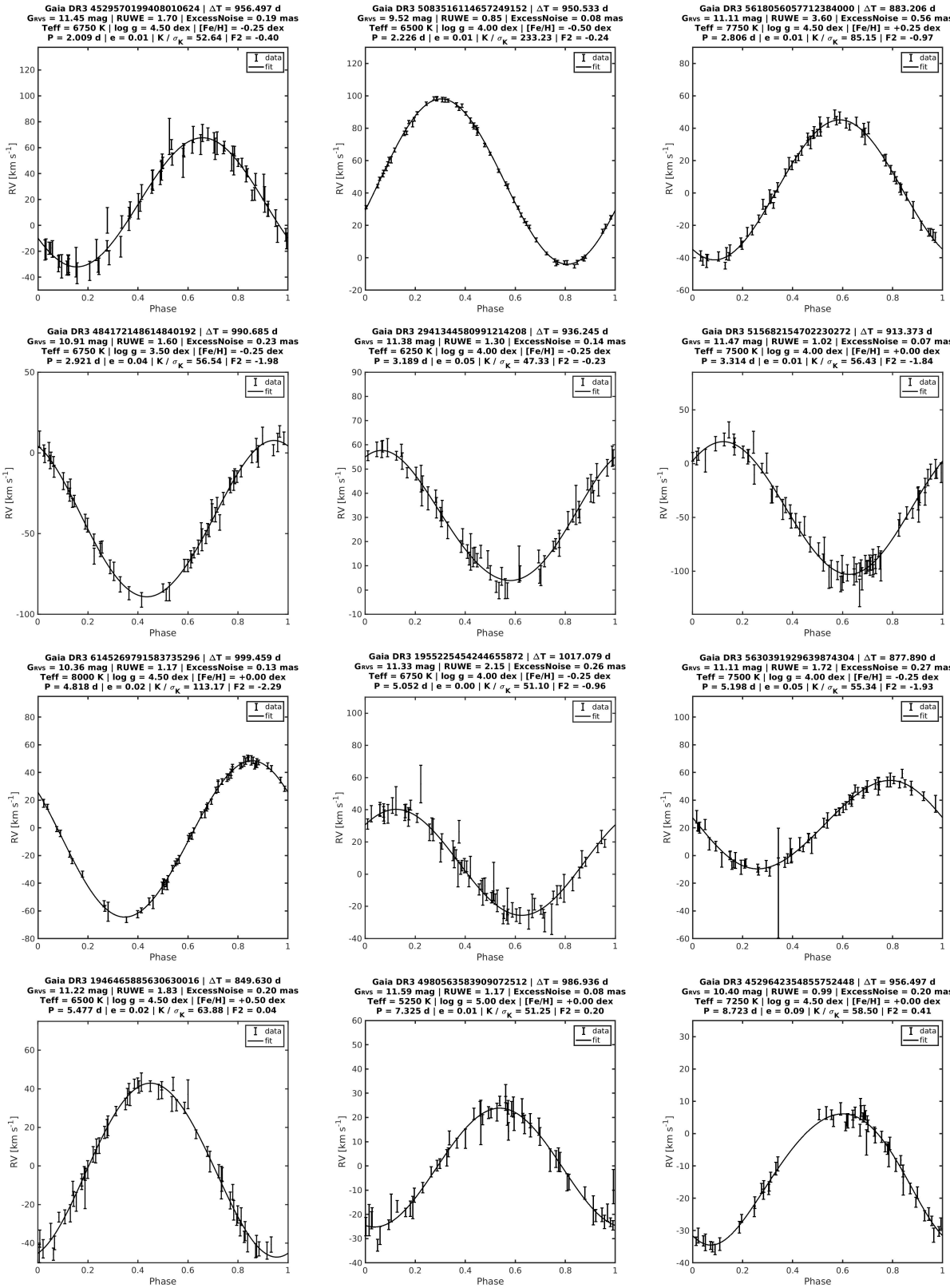

Fig. E.1: Good results: a few examples illustrative of the output of the pipeline for SB1-type solutions. Each panel concerns an object whose *Gaia* name is given in the header. Each of the panels shows the phase diagram containing the folded RVs (data points at the centre of the $\pm 1\sigma$ error bars) along with the fitted orbital solution. The header gives also the time span covered by the time-series (ΔT). The second line gives the $G_{\rm RVS}^{\rm int}$ magnitude of the object, the astrometric `ruwe` and the astrometric excess noise, whereas the third line concerns the physical parameters identifying the template used. The last line indicates the period, the eccentricity, the significance, and the statistic F_2 related to the adopted solution. The objects are ordered by increasing period.

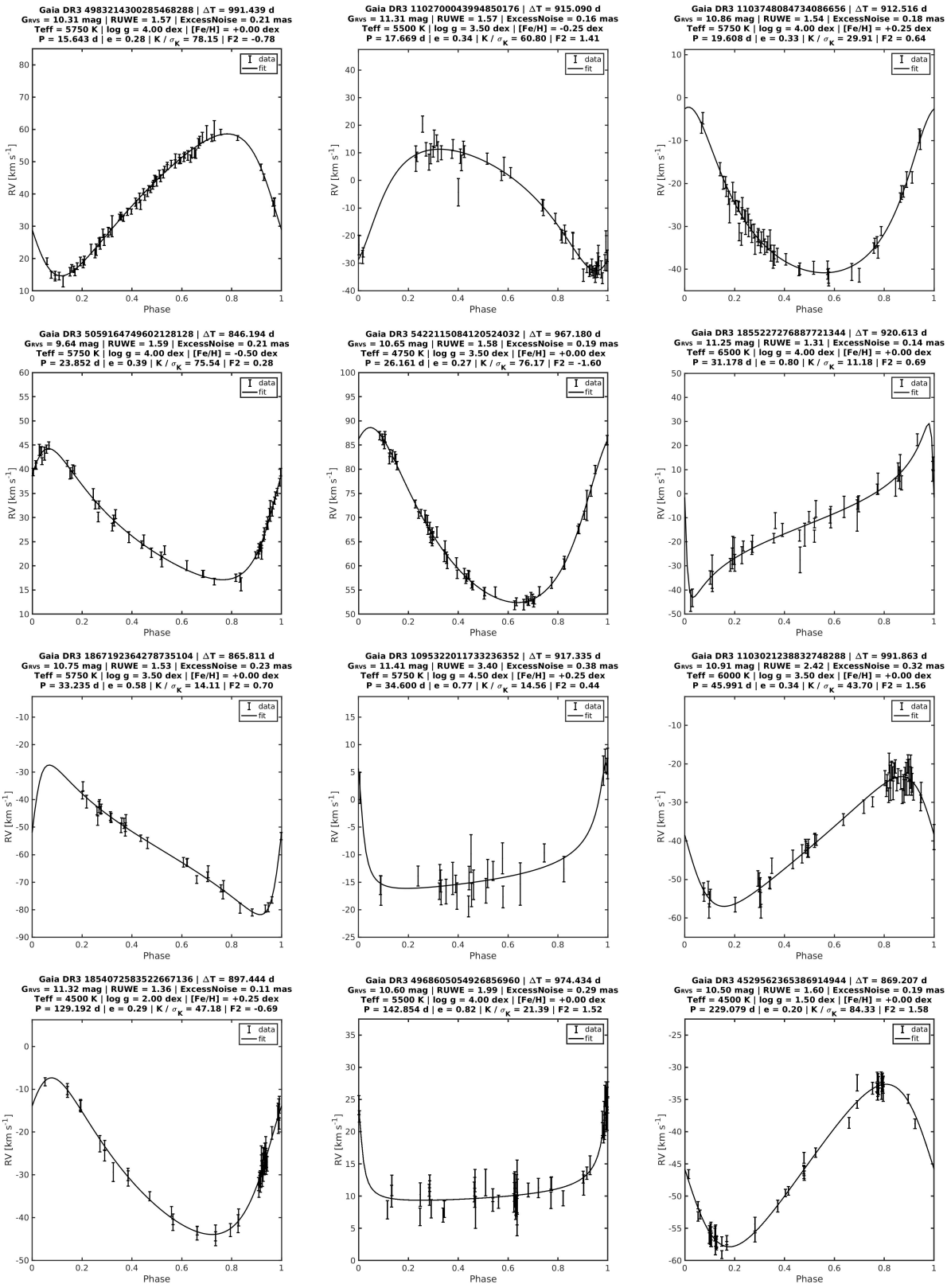

Fig. E.1: continued.

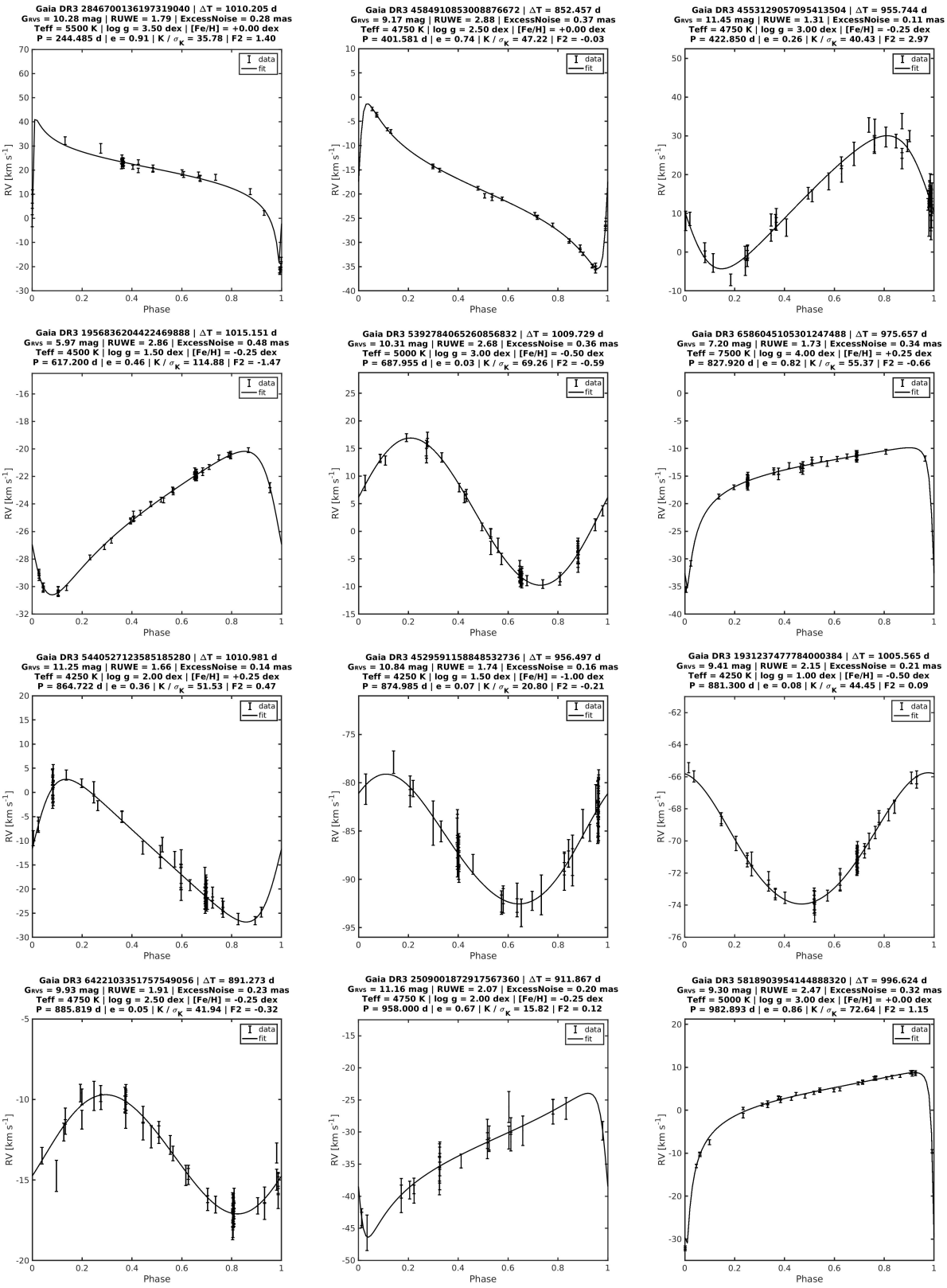

Fig. E.1: continued.

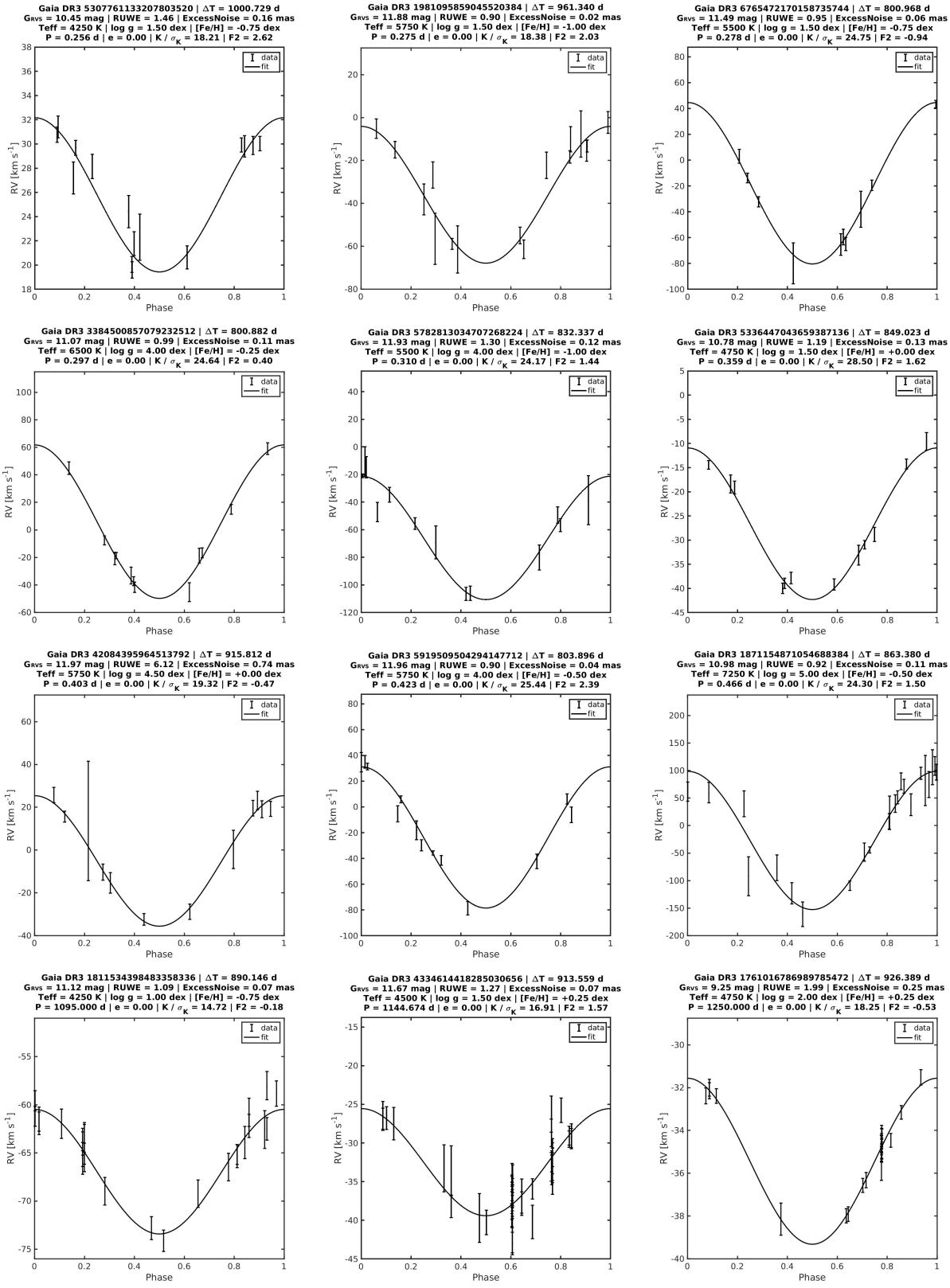

Fig. E.2: Good results: same as Fig. E.1 but concerning the SB1C-type solutions.

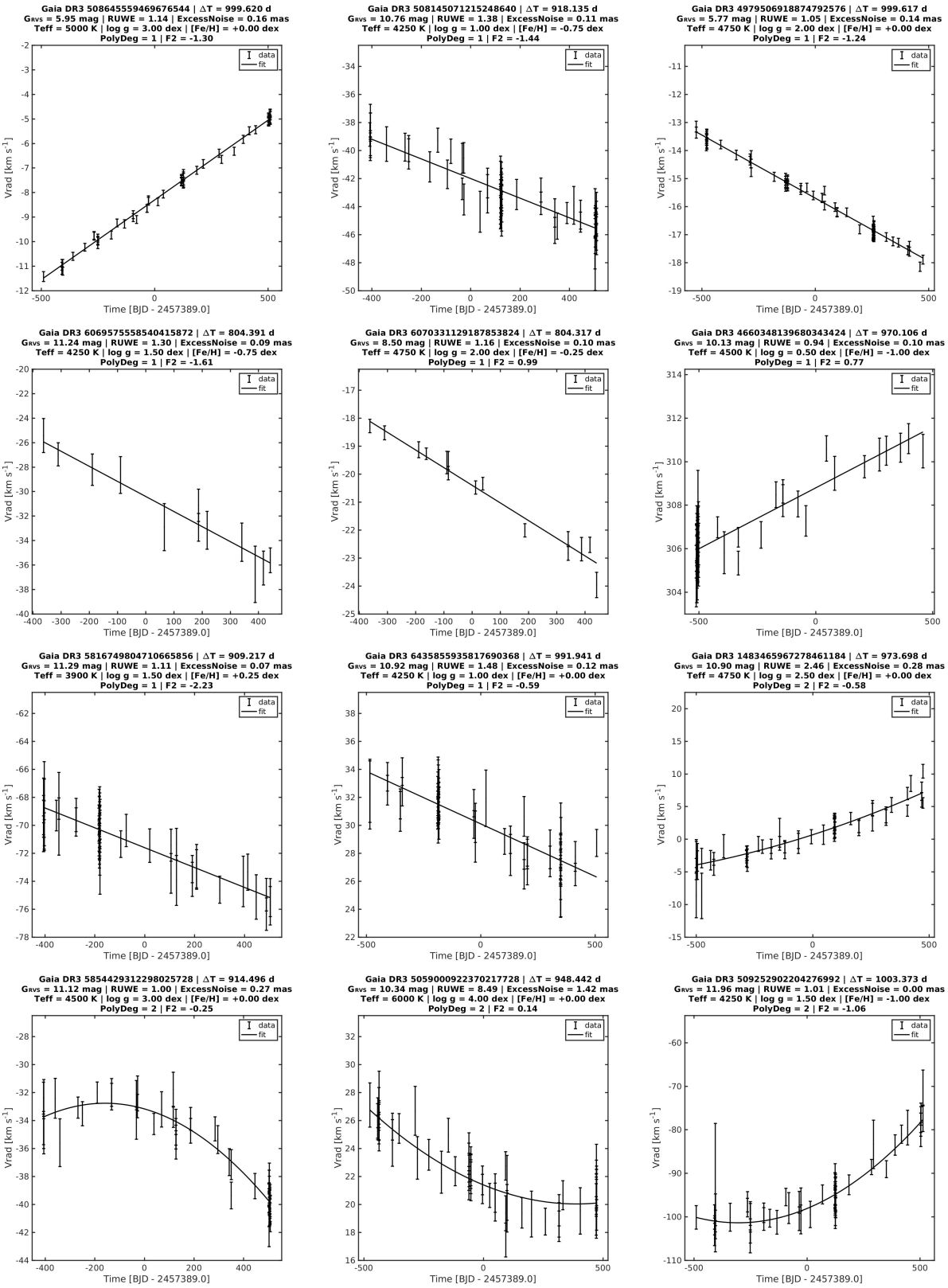

Fig. E.3: Good results: same as Fig. E.1 but concerning the TrendSB1-type solutions. The order of the objects is arbitrary, except that the second degree trends have been placed at the end.

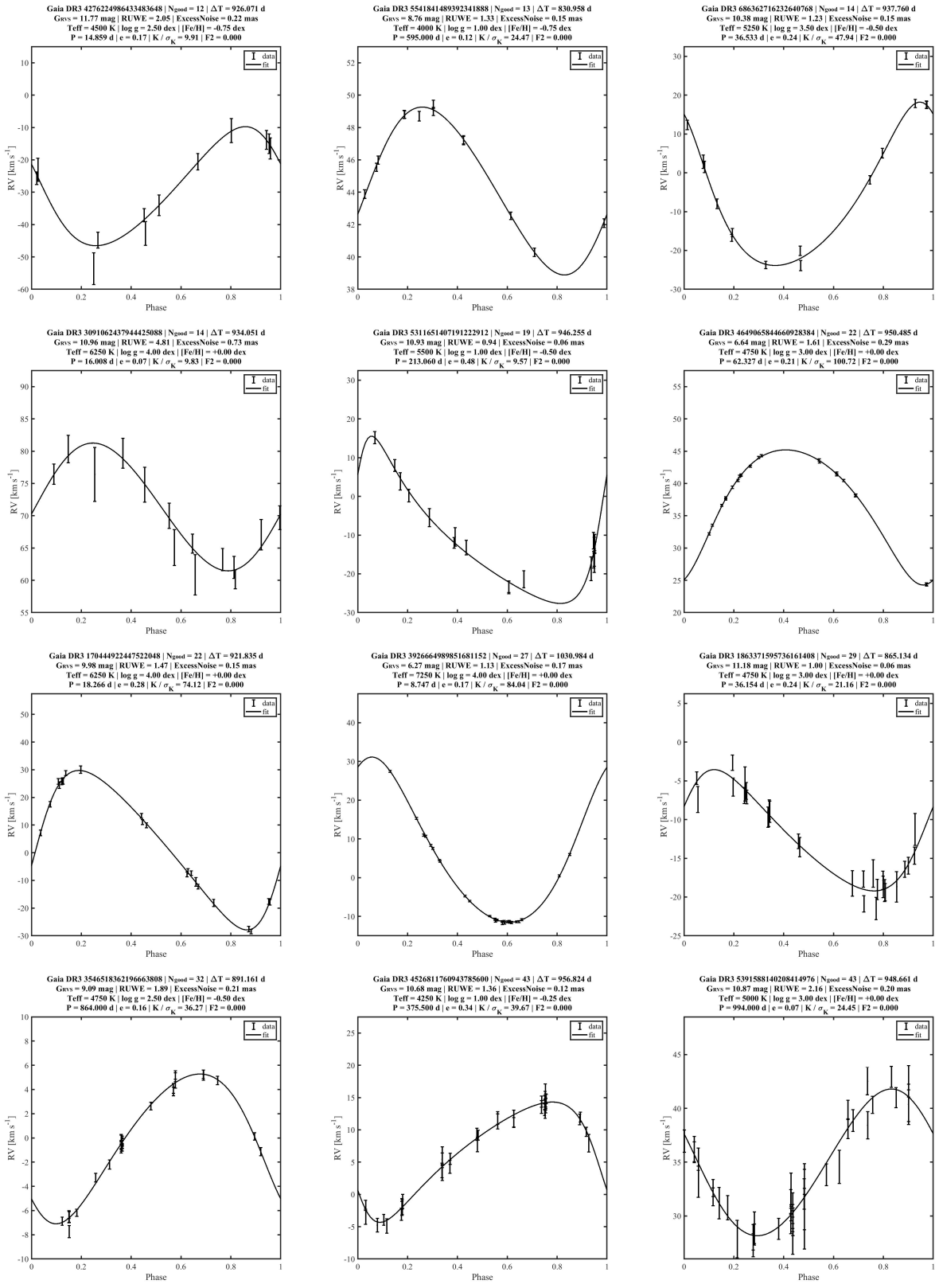

Fig. E.4: This figure exhibits the RV curves and the SB1 orbital solutions for a random sample of objects from the catalogue. All the solutions have a similar F_2 around zero but have otherwise been selected at random with $N_{\rm good}$ comprised between 10 and 45. They have been ordered by increasing $N_{\rm good}$. The case of larger number of data points has already been illustrated in Fig. E.1.

Appendix F: Comparison of orbital parameters with respect to literature values

Figures illustrating the deviations in P (expressed in σ units) with respect to external catalogues are shown in Sect. 9.4 as a function of the reference period. Here we extend such comparisons to other orbital parameters (e, γ, and K) and show the dependence with other relevant quantities (including the P from our catalogue, not the reference one).

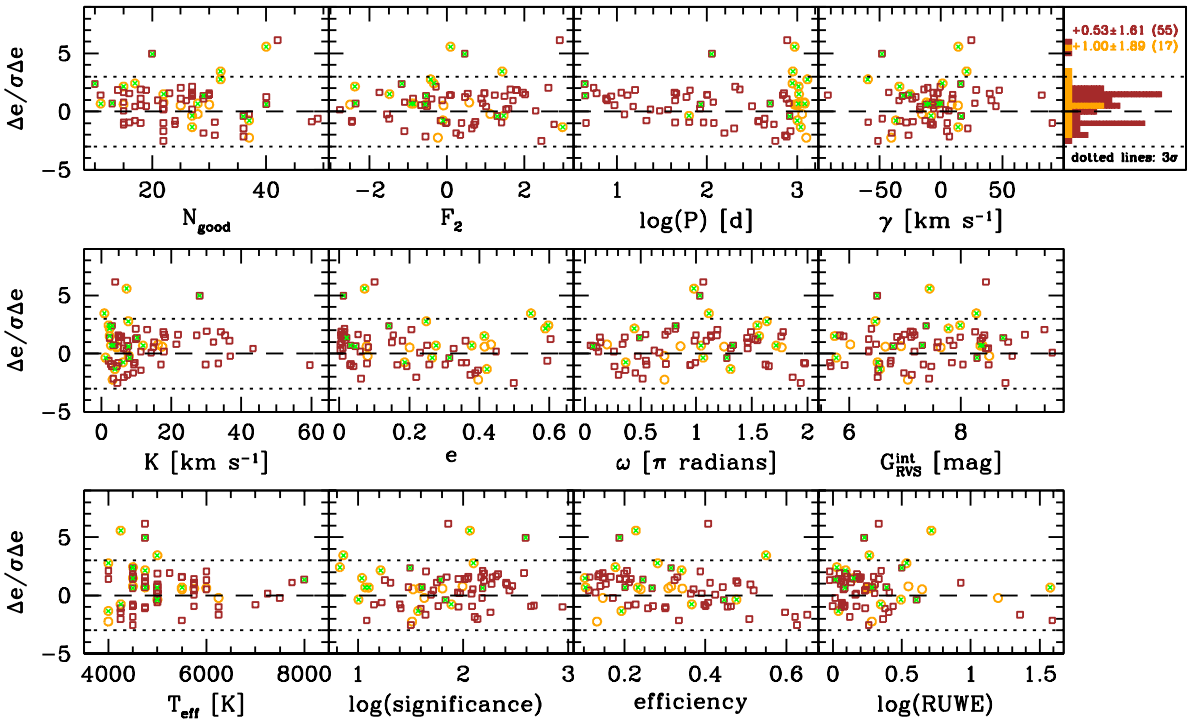

Fig. F.1: Comparison for the eccentricity, e, between the DR3 spectroscopic values and those determined by Griffin and collaborators. Systems for which the period, P, in the literature is unlikely to be found (i.e. $\Delta T < P$) are indicated with orange circles. Systems for which $\Delta T \geqslant P$ are shown as brown squares. Binaries for which the reference period is not recovered to within 3σ are flagged with green crosses. The quantity $T_{\rm eff}$ refers to the effective temperature of the template used to determine the RVs (Katz et al. 2023).

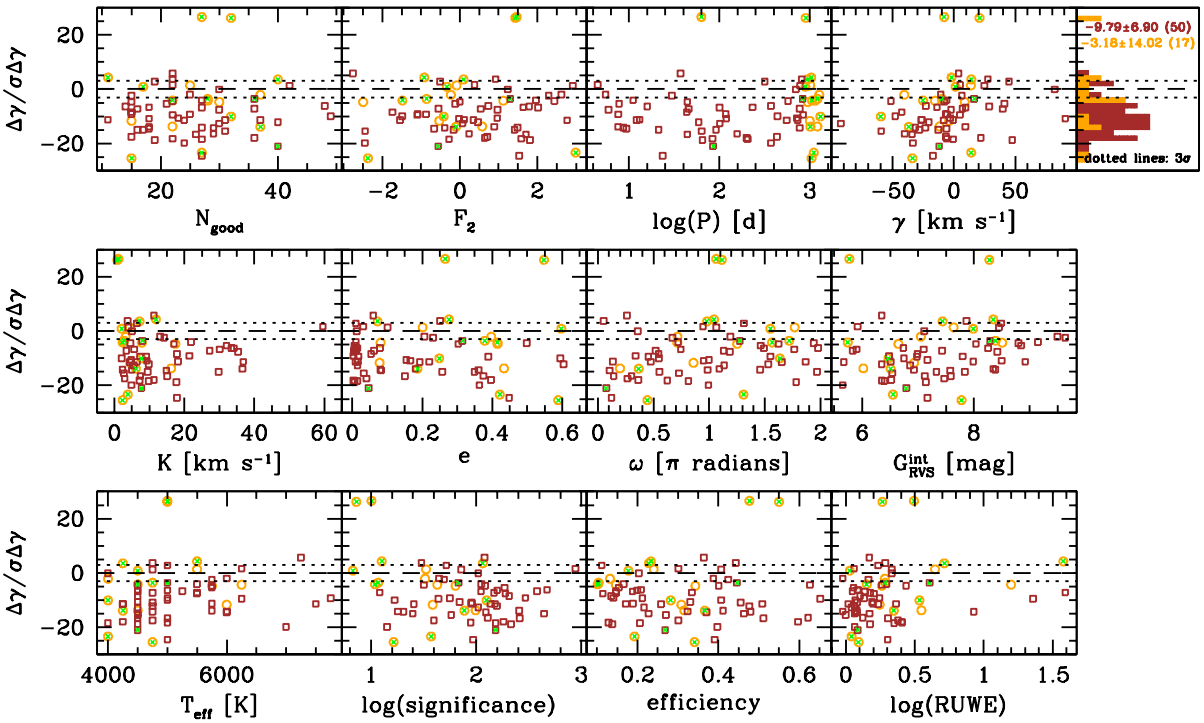

Fig. F.2: Same as Fig. F.1 in the case of Griffin, but for γ.

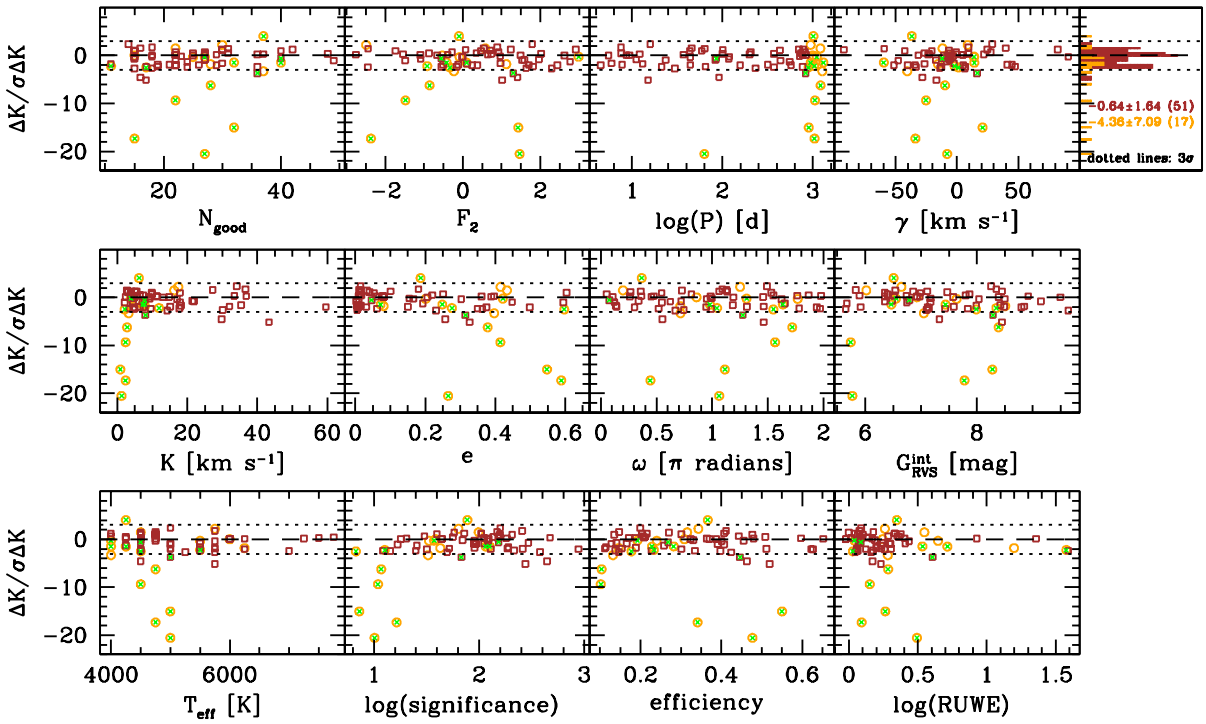

Fig. F.3: Same as Fig. F.1 in the case of Griffin, but for K.

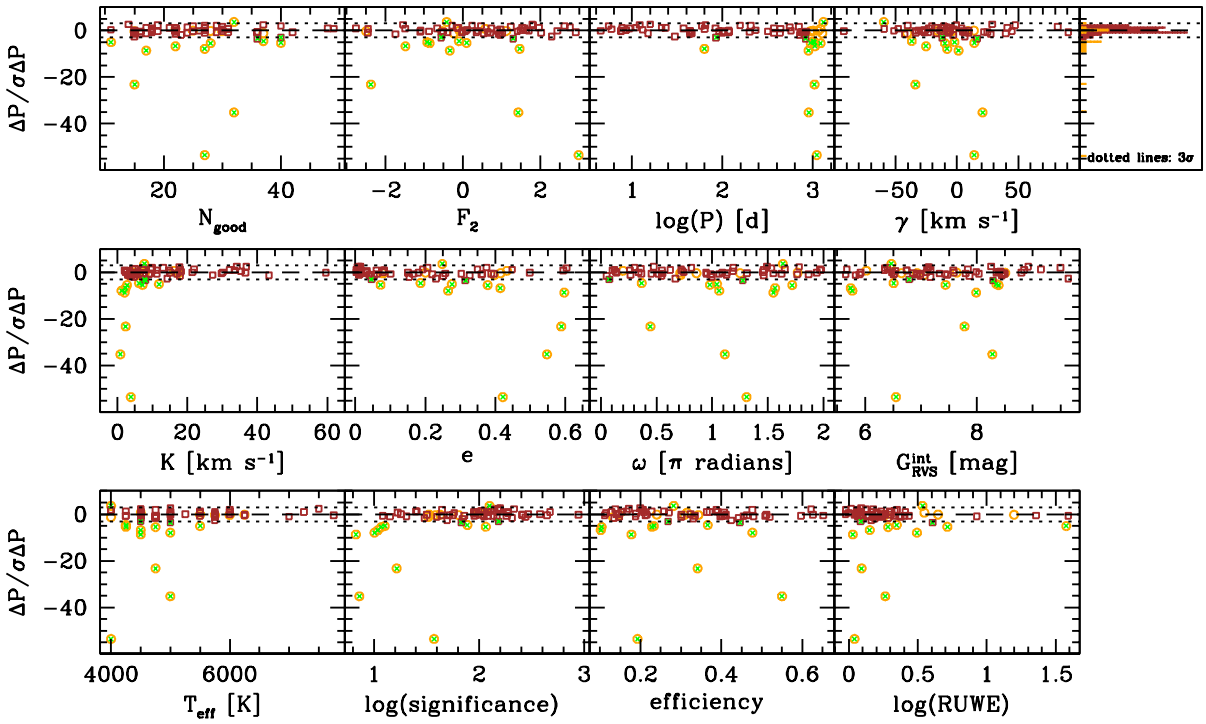

Fig. F.4: Same as Fig. F.1 in the case of Griffin, but for P.

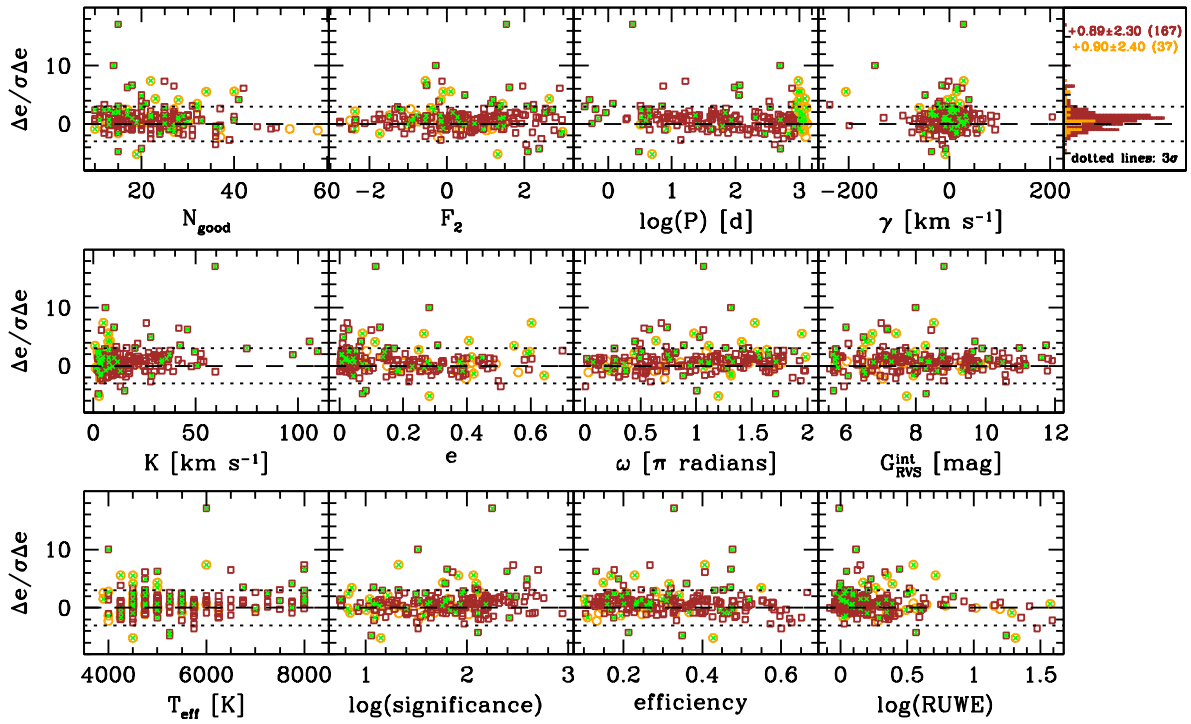

Fig. F.5: Comparison for the eccentricity, e, between the DR3 spectroscopic values and those in the SB9. Systems for which the period, P, in the literature is unlikely to be found (i.e. $\Delta T < P$) are indicated with orange circles. Systems for which $\Delta T \geqslant P$ are shown as brown squares. Binaries for which the reference period is not recovered to within 3σ are flagged with green crosses. The quantity $T_{\rm eff}$ refers to the effective temperature of the template used to determine the RVs (Katz et al. 2023).

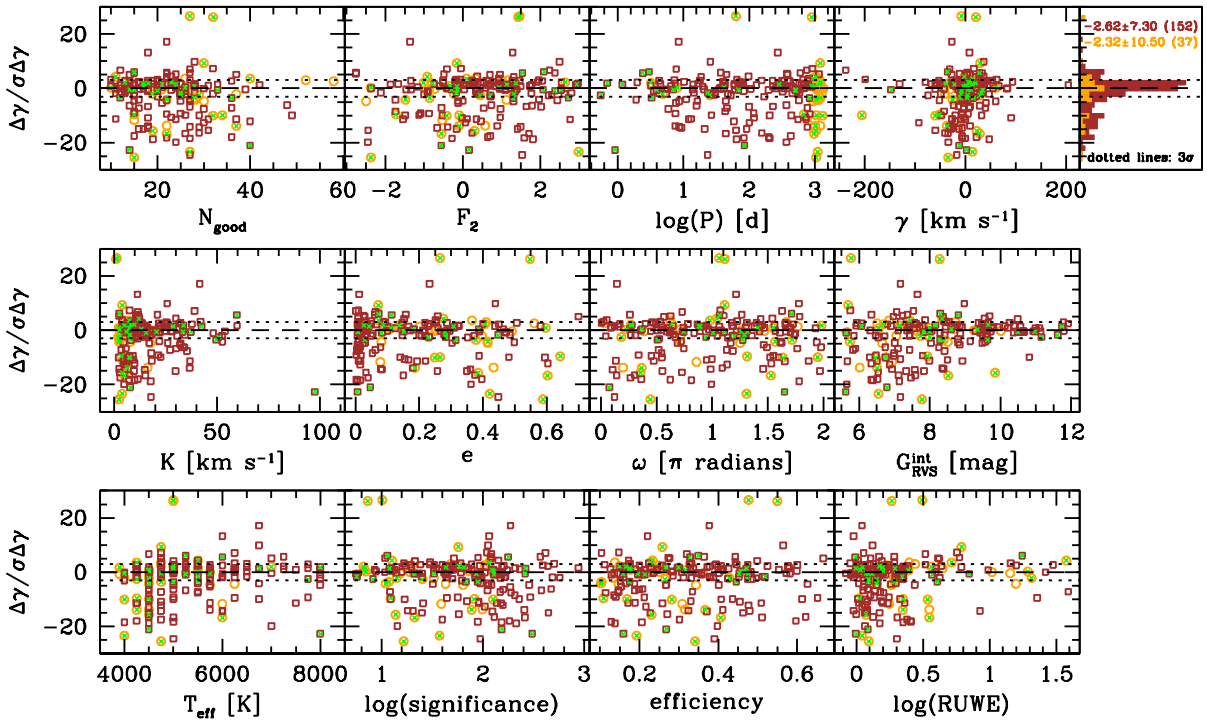

Fig. F.6: Same as Fig. F.5 in the case of the SB9, but for γ.

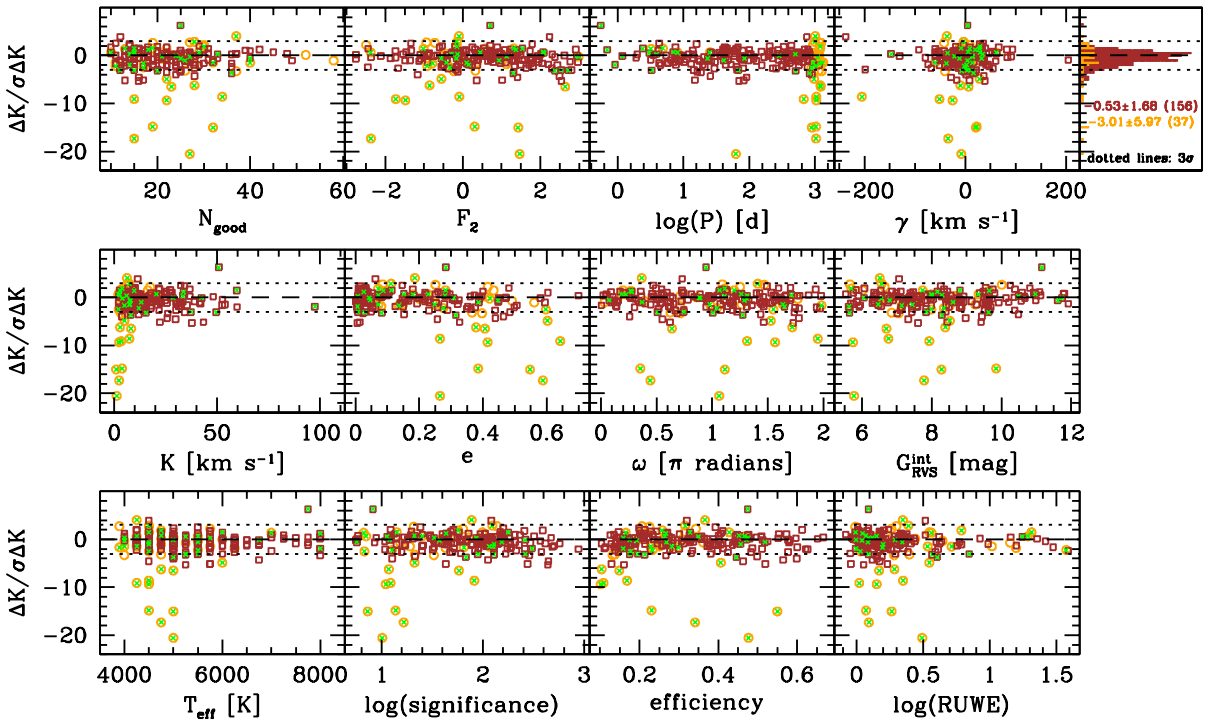

Fig. F.7: Same as Fig. F.5 in the case of the SB9, but for K.

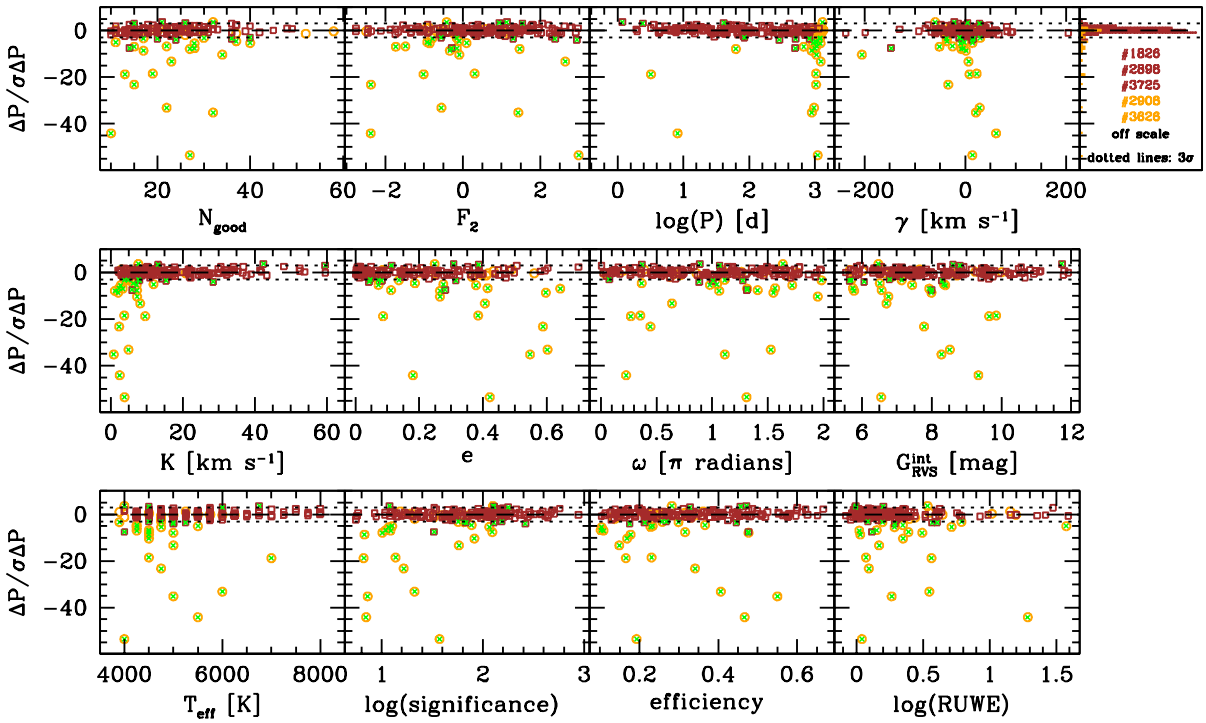

Fig. F.8: Same as Fig. F.5 in the case of the SB9, but for P. As indicated, a few systems have very negative $\Delta P/\sigma\Delta P$ values and are off scale. The SB9 IDs are given.

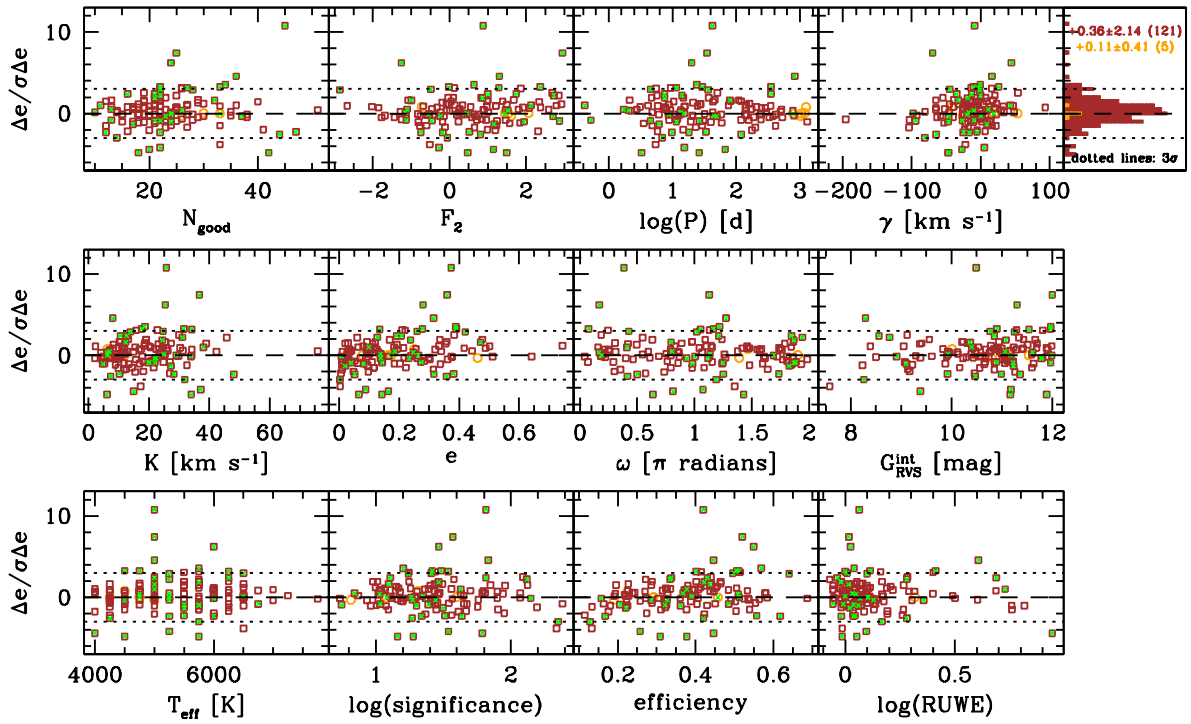

Fig. F.9: Comparison for the eccentricity, e, between the DR3 spectroscopic values and those in PW20. Systems for which the period, P, in the literature is unlikely to be found (i.e. $\Delta T < P$) are indicated with orange circles. Systems for which $\Delta T \geqslant P$ are shown as brown squares. Binaries for which the reference period is not recovered to within 3σ are flagged with green crosses. The quantity $T_{\rm eff}$ refers to the effective temperature of the template used to determine the RVs (Katz et al. 2023).

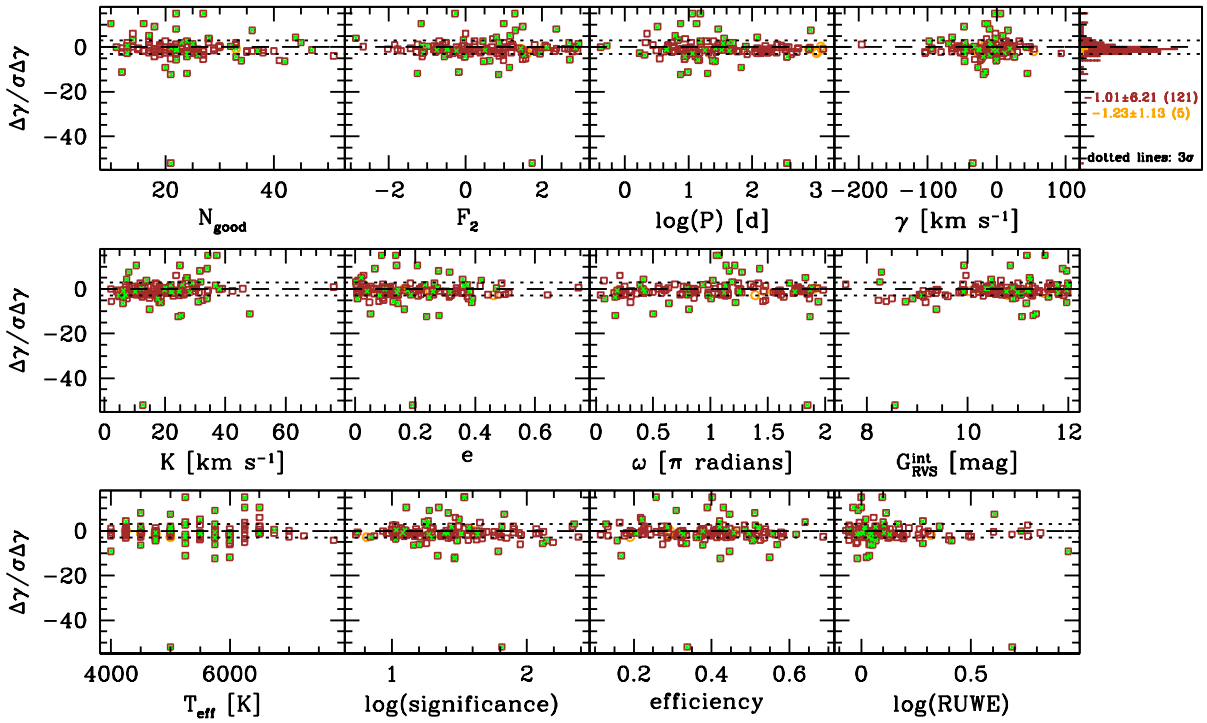

Fig. F.10: Same as Fig. F.9 in the case of PW20, but for γ.

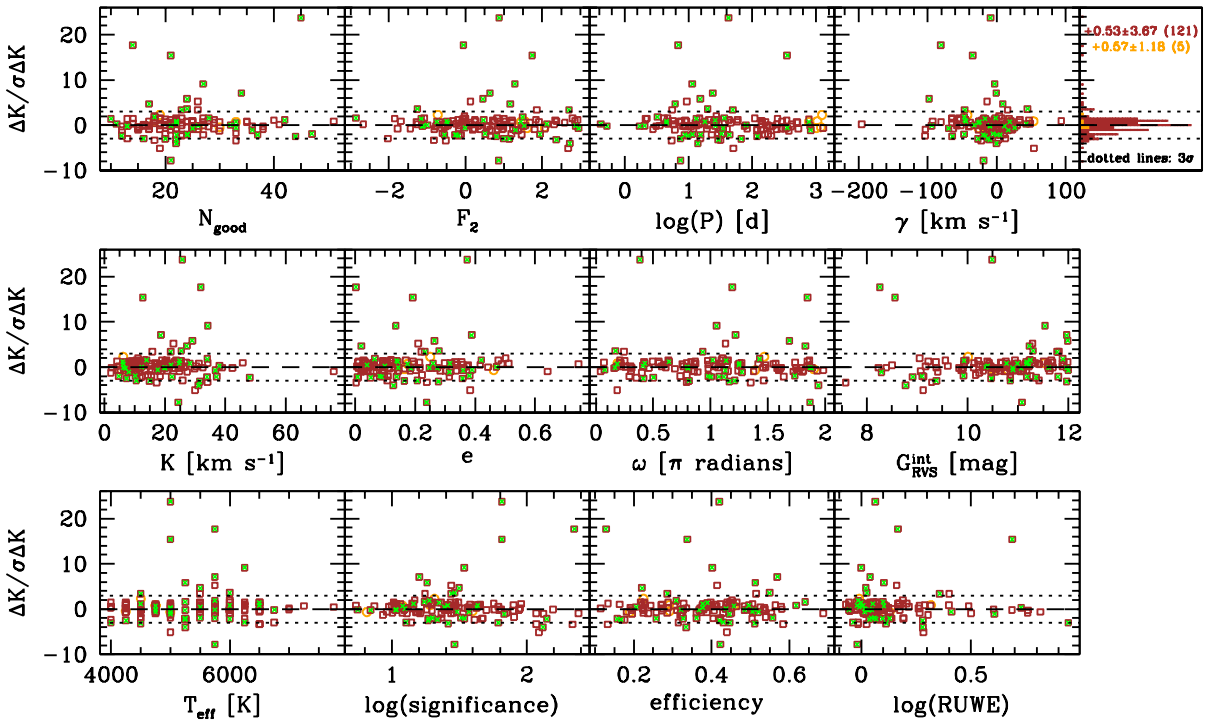

Fig. F.11: Same as Fig. F.9 in the case of PW20, but for the semi-amplitude K.

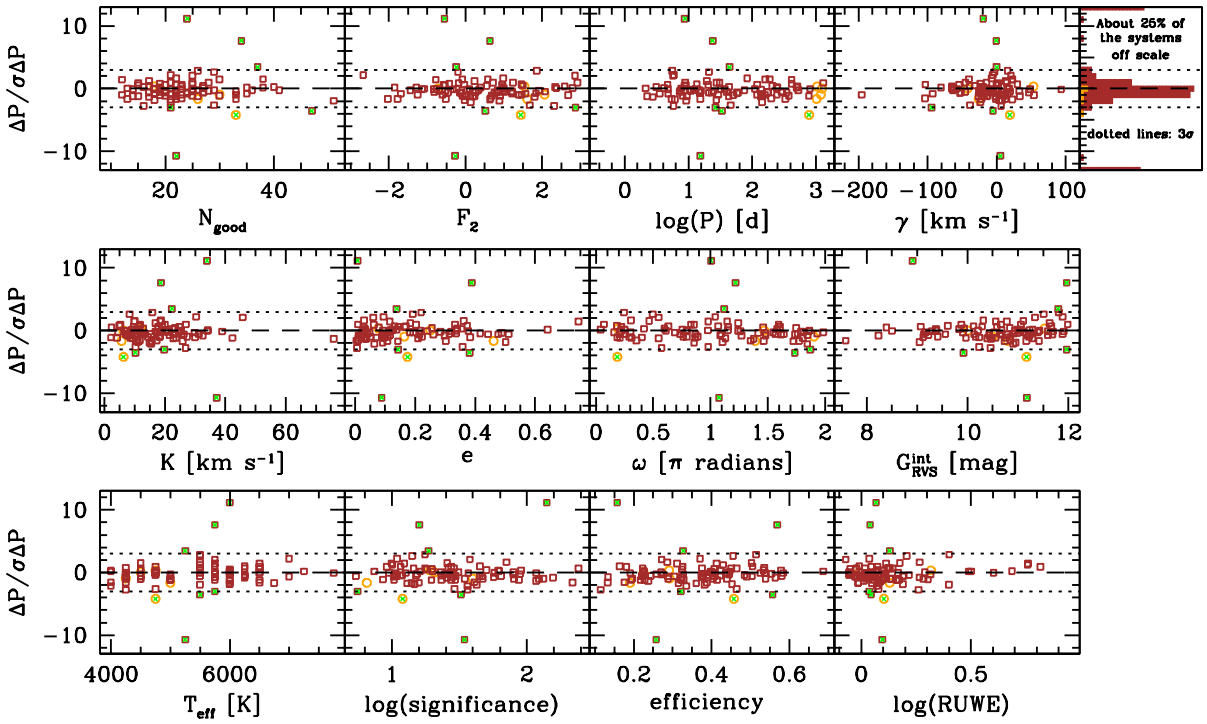

Fig. F.12: Same as Fig. F.9 in the case of PW20, but for P. We note that a significant number of systems are off scale.

Appendix G: Processing steps and outcome of analysis for SB9 systems

As for Griffin's catalogue, the small number of SB9 systems eventually retained for validation (Sect. 9.4.2 and Figs. F.5- F.8) arises from the use of only a subset of the reference data set, along with the numerous selection criteria applied to the DR3 data described in Tables 2, 3, 4 and H.4. Figure G.1 provides a summary of the various cuts that were applied, along with the number of SB9 sources remaining at each stage and the final outcome of the analysis of spectroscopic binaries by CU4/NSS.

- **Step 1: selection applied to the cross-matches with SB9**
  We start off with the 3323 cross-matches out of the 4021 binaries in the SB9. Among them, close to 30% are visual/multiple systems, and are rejected straight away from the input catalogue (see beginning of Sect. 9.4.1). Furthermore, a few objects have duplicated entries in the SB9.

- **Step 2: selection based on SB types in SB9**
  We did not consider further the SB2 solutions reported in SB9, which at this stage constitute ~25% of the reference sample. As for the previous step, of course, rejection for validation purposes of a given system does not preclude it entering the DR3 subcatalogue. Among the 1750 SB1 objects from SB9, 1476 (=1750-226-45-3) do not have spectroscopic deterministic solutions (Sect. 9.4.2).

- **Step 3: CU6 data not feeding the present pipeline**
  For more than half of the remaining systems, the CU6 data are either not transmitted to our pipeline for analysis or will not lead to any solutions. As discussed in Sects. 2 and 6.3.1, it is mainly because there is either no compelling evidence for variability in the RV time-series, there are not enough valid RV measurements, or the source lies outside the $G_{\rm RVS}^{\rm int}$ or $T_{\rm eff}$ ranges. We note that ~20% of the entries in the whole SB9 contain an OBA component.

- **Step 4: internal selection within our filtering scheme**
  Finally, only a relatively small fraction of the remaining sources have either a proposed `SB1`, `SB1C`, or `TrendSB1` solution as a result of the numerous quality cuts described in Sect. 7.1 (see also Tables 2, 3, 4 and H.4). As an example, Fig. G.2 gives full details about the internal filtering applied to the `TrendSB1` and `SB1` solution types. In addition, we recall that the cross-matches with the combined and `StochasticSB1` DR3 solutions are not counted in Sect. 9.4.2. The same holds for the purely astrometric orbital solutions or those for EBs only based on photometry.

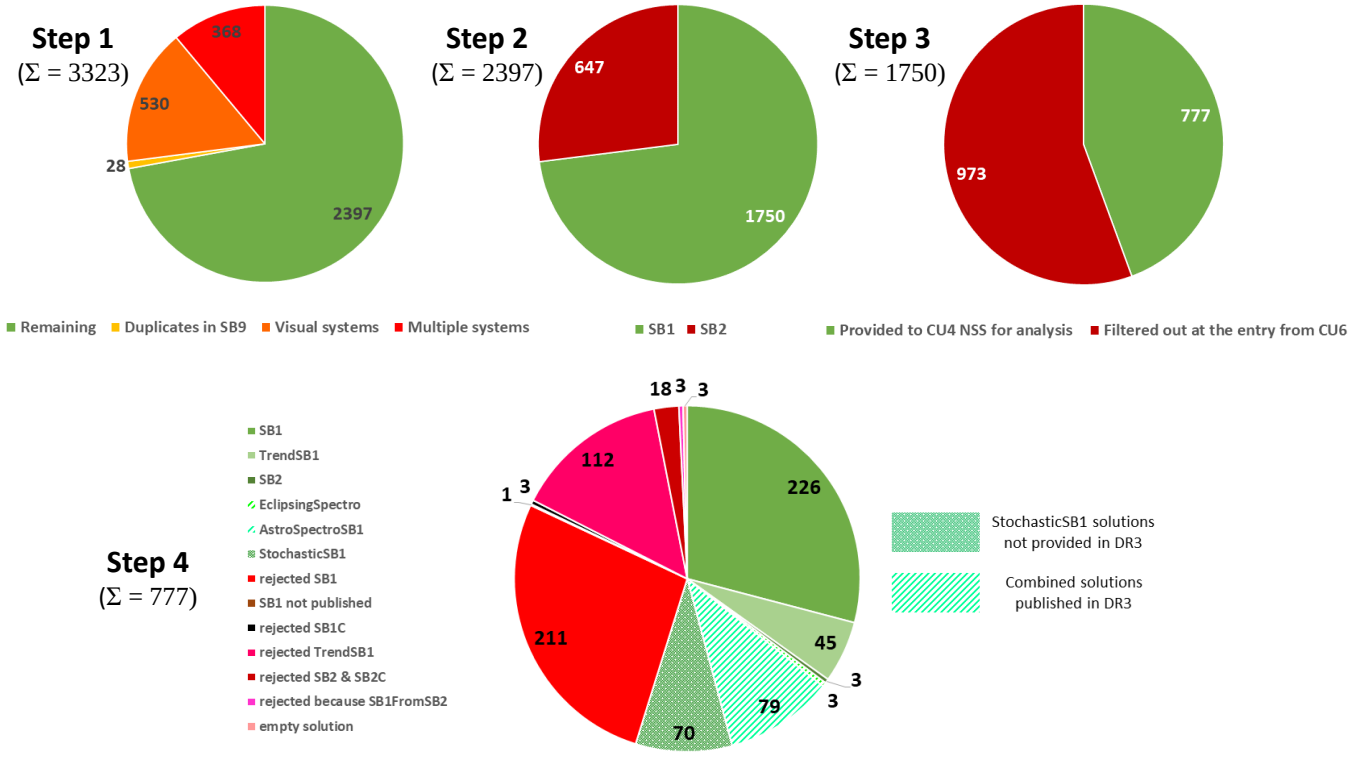

Fig. G.1: Overview of the cleaning of the input SB9 catalogue and processing history of the sources selected. The bottom pie chart shows the census of the results at the very end of the chain. The sources that received an empty solution ended up with an insufficient number of valid RV measurements after removal of the outliers. Indicated as "not published" is Gaia DR3 2178837257167184896, which is among the 94 systems discussed in Sect. 8.1, and does not have neither an `SB1` nor a combined solution in DR3.

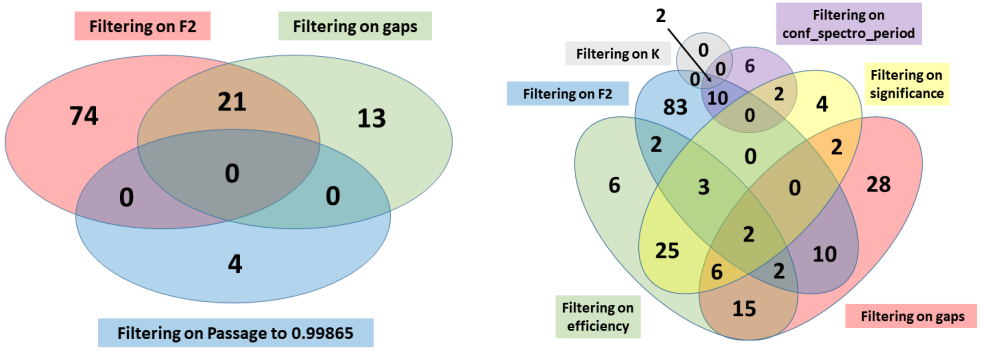

Fig. G.2: Venn diagrams describing the internal filtering that led to the rejection of 112 `TrendSB1` (left) and 211 `SB1` (right) solutions in DR3, respectively. In the latter case, three systems with multiple flags have been omitted for clarity.

Appendix H: Parameters delivered to the catalogue for classes SB1, SB1C and TrendSB1.

Table H.1 lists the parameters computed in the present work concerning the SB1 class. Table H.2 deals with the SB1C class and Table H.3 with the TrendSB1 one. Table H.4 summarises the selection criteria applied on the way to the SB-subcatalogue.

Table H.1: List of the parameters delivered by the present work concerning the SB1 class. The first column gives the parameter name, column 2 the relevant symbol used here. The third column offers the name of the entry in the catalogue itself. The fourth column gives the type of the computer variable in the catalogue, and column 5 the physical units used. The last column contains any remark.

Parameter	Symbol	Table entry	Type	Units	Remarks
Solution type	SB1	nss_solution_id	string	-	
Orbital period	P	period	double	d	
Uncertainty	σ_P	period_error	float	d	
Systemic velocity	γ	center_of_mass_velocity	double	km s^{-1}	
Uncertainty	σ_γ	center_of_mass_velocity_error	float	km s^{-1}	
Semi-amplitude	K	semi_amplitude_primary	double	km s^{-1}	
Uncertainty	σ_K	semi_amplitude_primary_error	float	km s^{-1}	
Eccentricity	e	eccentricity	double	none	
Uncertainty	σ_e	eccentricity_error	float	none	
Argument of periastron	ω	periastron_argument	double	degree	radian (this work)
Uncertainty	σ_ω	periastron_argument_error	float	degree	
Periastron epoch	T_0	t_periastron	double	Barycentric JD	
Uncertainty	σ_{T_0}	t_periastron_error	float	Barycentric JD	
Total number of points	$N_{\rm tot}$	rv_n_obs_primary	integer	none	
Total number of valid points	$N_{\rm good}$	rv_n_good_obs_primary	integer	none	
Objective function	χ^2	obj_function	double	none	
Goodness of fit	F_2	goodness_of_fit	float	none	
Efficiency	-	efficiency	float	none	
Significance	K/σ_K	significance	float	none	
Flags	-	flags	long	-	see appendix I
Confidence on period	-	conf_spectro_period	float	-	
Concerned parameters	-	bit_index	long	-	$\equiv$ 127
Vector of correlations	-	corr_vec (length 15)	float	-	

Table H.2: Same as Table H.1 but for the SB1C class.

Parameter	Symbol	Table entry	Type	Units	Remarks
Solution type	SB1C	nss_solution_id	string	-	
Orbital period	P	period	double	d	
Uncertainty	σ_P	period_error	float	d	
Systemic velocity	γ	center_of_mass_velocity	double	km s^{-1}	
Uncertainty	σ_γ	center_of_mass_velocity_error	float	km s^{-1}	
Semi-amplitude	K	semi_amplitude_primary	double	km s^{-1}	
Uncertainty	σ_K	semi_amplitude_primary_error	float	km s^{-1}	
Maximum velocity epoch	T_0	t_periastron	double	Barycentric JD	entry misleading
Uncertainty	σ_{T_0}	t_periastron_error	float	Barycentric JD	entry misleading
Total number of points	$N_{\rm tot}$	rv_n_obs_primary	integer	none	
Total number of valid points	$N_{\rm good}$	rv_n_good_obs_primary	integer	none	
Objective function	χ^2	obj_function	double	none	
Goodness of fit	F_2	goodness_of_fit	float	none	
Efficiency	-	efficiency	float	none	
Significance	K/σ_K	significance	float	none	
Flags	-	flags	long	-	see appendix I
Confidence on period	-	conf_spectro_period	float	-	
Concerned parameters	-	bit_index	long	-	$\equiv$ 31
Vector of correlations	-	corr_vec (length 6)	float	-	

Table H.3: Same as Table H.1 but for the `TrendSB1` class.

Parameter	Symbol	Table entry	Type	Units	Remarks
Solution type	First DegreeTrendSB1 SecondDegreeTrendSB1	`nss_solution_id`	string	-	
Mean velocity	V_0	`mean_velocity`	double	$\mathrm{km\,s^{-1}}$	
Uncertainty	σ_{V_0}	`mean_velocity_error`	float	$\mathrm{km\,s^{-1}}$	
First order derivative	$\frac{\partial V}{\partial t}$	`first_deriv_velocity`	double	$\mathrm{km\,s^{-1}\,d^{-1}}$	
Uncertainty	$\sigma_{\frac{\partial V}{\partial t}}$	`first_deriv_velocity_error`	float	$\mathrm{km\,s^{-1}\,d^{-1}}$	
Second order derivative	$\frac{\partial^2 V}{\partial t^2}$	`second_deriv_velocity`	double	$\mathrm{km\,s^{-1}\,d^{-2}}$	
Uncertainty	$\sigma_{\frac{\partial^2 V}{\partial t^2}}$	`second_deriv_velocity_error`	float	$\mathrm{km\,s^{-1}\,d^{-2}}$	
Total number of points	N_{tot}	`rv_n_obs_primary`	integer	none	
Total nbr of valid points	N_{good}	`rv_n_good_obs_primary`	integer	none	
Objective function	χ^2	`obj_function`	float	none	
Goodness of fit	F_2	`goodness_of_fit`	float	none	
Flags	-	`flags`	long	-	appendix I
Concerned parameters	-	`bit_index`	long	-	$\equiv$ 7 or 15
Vector of correlations	-	`corr_vec` (length 1 or 3)	float	-	

Table H.4: Summary of the various selection criteria applied at various stages on the way to the SB-subcatalogue (classes `SB1` and `SB1C`).

Stage of application	Selection criterion	Description in
Transfer from CU6 products	RV time-series available	Katz et al. (2023)
	Normal stars, no spectral peculiarities	Katz et al. (2023)
	Object not classified as SB2	Damerdji et al. (2024)
Selection of objects/time-series at entry	`rv_renormalized_gof` larger than 4	Sect. 2
	T_{eff} in [3875 - 8125] K	Sect. 2
	$G^{\mathrm{int}}_{\mathrm{RVS}}$ mag in [5.5 - 12]	Sect. 2
	`rv_chisq_pvalue` less than or equal to 0.01	Sect. 2
	RV outlier rejected from time-series	Sect. 6.3.1
	N_{good} larger than or equal to 10	Sect. 6.3.1
Internal filtering on solutions	$\lvert\gamma\rvert \leq 1000\ \mathrm{km\,s^{-1}}$	Sect. 7.1
	F_2 less than or equal to 3	Sect. 7.1
	Rejection of solutions with bad flags	Sect. 7.1
	K less than or equal to 250 $\mathrm{km\,s^{-1}}$	Sect. 7.1
	`efficiency` greater than or equal to 0.1	Sect. 7.1
	$\delta\phi$ less than or equal to 0.3	Sect. 7.1
	`conf_spectro_period` { - ≥ 0.95 if $P \geq 10$ d; - ≥ 0.995 if $P \leq 1$ d; - $\geq 0.995 - 0.045\times \log P$ in between }	Sect. 7.1
	`significance` larger than or equal to 5	Sect. 7.1
	σ_ω less than 2π (solely for SB1)	Sect. 7.1
Loss by combination	—	Sect. 7.2
Post-filtering	380 objects rejected as intrinsic variables (Cepheids and RR Lyrae)	Sect. 10.1.1
	1475 objects rejected having more than 10 % double-line transits	Sect. 10.1.2
	164 objects rejected suffering from a scan-angle effect	Sect. 10.1.3

Appendix I: Various flags linked to the processing

Table I.1 details the various flags that could be activated during the spectroscopic orbital solution processing, along with the relevant explanations in the framework of the decision tree.

Table I.1: This table is the repertory of the various flags utilised in the chain.

Flag bit nr.	Value	Logical Variable
8	256	BAD_UNCHECKED_NUMBER_OF_TRANSITS
Explanation: The number of transits is not sufficient to process the star (before removing bad transits)		
9	512	NO_MORE_VARIABLE_AFTER_FILTERING
Explanation: The RV curve is no more variable after velocity filtering (at the threshold 0.9)		
10	1024	BAD_CHECKED_NUMBER_OF_TRANSITS
Explanation: The number of transits is not sufficient to process the star (after removing bad transits)		
11	2048	SB2_REDIRECTED_TO_SB1_CHAIN_NOT_ENOUGH_COUPLE_MEASURES
Explanation: SB2 is redirected to the SB1 chain because there are not enough couples of measures		
12	4096	SB2_REDIRECTED_TO_SB1_CHAIN_PERIODS_NOT_COHERENT
Explanation: SB2 is redirected to the SB1 chain because the periods found by the SB1 and SB2 chains are not coherent		
13	8192	NO_SIGNIFICANT_PERIOD_CAN_BE_FOUND
Explanation: No significant period can be derived (no period from photometric variability analysis and periodogram peaks below the cut-off threshold)		
14	16384	REFINED_SOLUTION_DOES_NOT_CONVERGE
Explanation: The refined orbital solution does not converge (after 1000 iterations)		
15	32768	REFINED_SOLUTION_SINGULAR_VARIANCE_COVARIANCE_MATRIX
Explanation: The variance-covariance matrix can not be obtained (singular) for the refined solution		
16	65536	CIRCULAR_SOLUTION_SINGULAR_VARIANCE_COVARIANCE_MATRIX
Explanation: The variance-covariance matrix can not be obtained (singular) for the circular solution		
17	131072	TREND_SOLUTION_SINGULAR_VARIANCE_COVARIANCE_MATRIX
Explanation: The variance-covariance matrix can not be obtained (singular) for the trend solution		
18	262144	REFINED_SOLUTION_NEGATIVE_DIAGONAL_OF_VARIANCE_COVARIANCE_MATRIX
Explanation: The diagonal of the variance-covariance matrix is negative for the refined solution		
19	524288	CIRCULAR_SOLUTION_NEGATIVE_DIAGONAL_OF_VARIANCE_COVARIANCE_MATRIX
Explanation: The diagonal of the variance-covariance matrix is negative for the circular solution		
20	1048576	TREND_SOLUTION_NEGATIVE_DIAGONAL_OF_VARIANCE_COVARIANCE_MATRIX
Explanation: The diagonal of the variance-covariance matrix is negative for the trend solution		
21	2097152	CIRCULAR_SOLUTION_DOES_NOT_CONVERGE
Explanation: The Lucy refined orbital solution diverges (after 1000 iterations)		
22	4194304	LUCY_TEST_APPLIED
Explanation: The Lucy test has been applied		
23	8388608	TREND_SOLUTION_NOT_APPLIED
Explanation: The trend analysis has not been applied (case of unsorted SB2)		
24	16777216	SOLUTION_OUTSIDE_E_LOGP_ENVELOP
Explanation: The orbital solution is above the e - log P envelop		
25	33554442	PERIOD_FOUND_IN_CU7_PERIODICITY
Explanation: The period is equal to a period issued from the CU7 (within the quadratic sum of their uncertainties)		
26	67108864	FORTUITOUS_SB2
Explanation: The RV1 and RV2 seem to be uncorrelated (contrary to the case of any binary system)		

Appendix J: Examples of retrieving a gold sample

– For an SB1 gold sample, we suggest limiting the efficiency to values larger than or equal to 0.2. To secure the determination of the periods and the subsequent fits, we advise adopting $N_{\rm good}$ larger or equal to 20. The most important selection is related to the significance that must remain larger or equal to 40. This condition eliminates dubious solutions, notably with small periods and large eccentricity. Solutions with periods larger than 800 d will not be secure, and are known over 1000 d to present biases and a small efficiency. Periods between 2 and 10 d can be kept thanks to the choice on the significance. An alternative possibility would be to relax the condition on the significance to 25-30 and to discard periods below 10 d. Below 2 d, we advise being cautious, although some positive validation took place. The following ADQL command will deliver some 15 314 objects:

```
SELECT * FROM gaiadr3.nss_two_body_orbit
WHERE nss_solution_type = 'SB1'
AND efficiency >= 0.2
AND rv_n_good_obs_primary >= 20
AND significance >=40
AND period <= 800
AND period >= 2 .
```

The recovery rate of the period for this gold sample reaches 93 %.

– Since objects characterised by a ruwe above 1.4 have thus a dubious position and consequently possible problems with the RVs, we recommend an additional selection on the astrometric ruwe. This selection implies the use of two tables and restricts the sample to 9578 objects:

```
SELECT * FROM gaiadr3.nss_two_body_orbit
INNER JOIN gaiadr3.gaia_source_lite USING (source_id)
WHERE nss_solution_type = 'SB1'
AND efficiency >= 0.2
AND rv_n_good_obs_primary >= 20
AND significance >=40
AND period <= 800
AND period >= 2
AND ruwe < 1.4 .
```

– Finally, we also present a gold selection on the linear trends that delivers 12 650 objects:

```
SELECT * FROM gaiadr3.nss_non_linear_spectro
WHERE nss_solution_type = 'FirstDegreeTrendSB1'
AND rv_n_obs_good_primary >= 20 .
```